

Exploitation of tannic acid as additive for the adhesion enhancement of UV-curable bio-based coating

*Original*

Exploitation of tannic acid as additive for the adhesion enhancement of UV-curable bio-based coating / Sesia, Rossella; Cardone, Anna Giulia; Ferraris, Sara; Spriano, Silvia; Sangermano, Marco. - In: PROGRESS IN ORGANIC COATINGS. - ISSN 0300-9440. - ELETTRONICO. - 189:(2024). [10.1016/j.porgcoat.2024.108311]

*Availability:*

This version is available at: 11583/2985771 since: 2024-02-07T15:59:12Z

*Publisher:*

Elsevier

*Published*

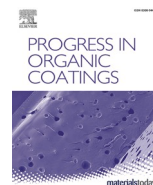
DOI:10.1016/j.porgcoat.2024.108311

*Terms of use:*

This article is made available under terms and conditions as specified in the corresponding bibliographic description in the repository

*Publisher copyright*

(Article begins on next page)



# Exploitation of tannic acid as additive for the adhesion enhancement of UV-curable bio-based coating

Rossella Sesia, Anna Giulia Cardone, Sara Ferraris, Silvia Spriano, Marco Sangermano<sup>\*</sup>

Politecnico di Torino, Dipartimento di Scienza Applicata e Tecnologia, C.so Duca Degli Abruzzi 24, 10129 Torino, Italy

## ARTICLE INFO

### Keywords:

Bio-based coating  
Photopolymerization  
Tannic acid  
Epoxidized soybean oil  
Adhesion

## ABSTRACT

The interest in environmentally friendly coatings is rising to substitute for the oil-derived materials in the coating industry. In the present study, natural tannic acid (TA) is investigated as an additive to an epoxidized soybean oil-based (ESO) coating. TA solutions in propylene carbonate at two different concentrations were prepared and added to an ESO matrix with different weight ratios. The UV-curing process of the coatings was deeply assessed through real-time Fourier Transform Infrared (FTIR) spectroscopy and Differential Scanning photo Calorimetry (photo-DCS). A significant increase in high epoxy group conversion, around 90 %, was achieved thanks to the activated monomer mechanism, which involves the TA polyphenols. This mechanism accelerated the photocrosslinking process, but reduced the coatings' crosslinking density, as demonstrated by the dynamic thermal mechanical analysis. The hardness of coatings containing the TA additive decreased, while the hydrophobicity of the surface coatings remained unchanged after the TA incorporation. Lastly, the adhesion of the UV-cured coating was evaluated on low-carbon steel substrates. An outstanding enhancement in adhesion property was provided by the TA additive, whose phenols not only participate in the photocrosslinking reaction but also coordinate iron on the steel surface. Moreover, the influence of two different steel surface pre-treatments, the pickling and plasma processes, on the coatings' adhesion strength was studied.

## 1. Introduction

Every year, the demand for synthetic polymer products rises, especially in the coatings industry, as well as the public knowledge of their negative effects. Indeed, the methods of coatings production frequently involve nonrenewable and oil-derived chemicals. The coating sector consumes >60 % of the world's production of epoxy resins, on which most petroleum-derived thermosetting polymers are based [1]. The main ingredient of the most conventional and widely used epoxy resins in industry is bisphenol A (BPA). However, this petroleum-based compound has been known to induce serious hazardous effects on human and ecological health [2–4]. Consequently, the development of sustainable coatings prepared from renewable resources in accordance with green chemistry principles is required to reduce environmental concerns and the negative impact of traditional coatings on human health. Among renewable and biodegradable sources, bio-based monomers from many different types of vegetable oils have been proposed as potential alternatives thanks to their highly reactive sites [5,6]. Indeed, the high number of double bonds in the triglycerides chemical structures can be

functionalized with epoxy groups, which are exploited for the cross-linking process [7].

Nevertheless, the development of new and environmentally friendly technologies, as well as the variation in the raw materials, also plays an important role. Indeed, the traditional curing processes release a large amount of volatile organic compounds (VOCs), that are harmful to human beings and pollute the environment. The photopolymerization of polymer coatings represents a sustainable process since it shows several advantages, such as fast curing speed, energy saving, and no VOCs emission [8–11]. The photocrosslinking reaction is performed under light irradiation via a chain-growth mechanism involving the propagation of either radicals or cations [8,12]. As cationic UV-curing polymerization does not require an inert atmosphere and can continue in the dark thanks to the long-lived species generated by the photoinitiator, it exhibits important benefits over the use of radical processes [8,12,13].

Crivello was the first to investigate the design of cationically photocrosslinkable monomers from bio-renewable sources, including epoxidized triglyceride oils [14,15]. Several plant oils have been investigated for this purpose [1,2,6,7,15–21], but soybean oil has been

<sup>\*</sup> Corresponding author.

E-mail address: [marco.sangermano@polito.it](mailto:marco.sangermano@polito.it) (M. Sangermano).

<https://doi.org/10.1016/j.porgcoat.2024.108311>

Received 23 November 2023; Received in revised form 12 January 2024; Accepted 31 January 2024

Available online 6 February 2024

0300-9440/© 2024 The Authors. Published by Elsevier B.V. This is an open access article under the CC BY license (<http://creativecommons.org/licenses/by/4.0/>).

extensively industrially used as an abundantly available, low-cost, and non-depletable resource [22]. Fig. 1a displays the chemical structure of epoxidized soybean oil used for the cationic photopolymerization.

Although coatings based on UV-curing and epoxidized vegetable oils show good adhesion on different substrates [15,23], adhesion enhancement has emerged as one of the important concerns for promoting the use of UV-curable coatings for steel [24]. The easiest, most cost-efficient, and most effective way to increase the adherence of a UV-curable coating to a metal surface is the incorporation of an adhesion promoter in the coating formulation [24–28]. An adhesion promoter is a compound able to act as a “bridge” between the coating and the substrate since it contains at least two types of active functional groups. One can react with the substrate surface and, the other can participate in the curing polymerization of the coating [27]. A large number of adhesion promoters, including silane coupling agents and phosphate esters, have been exploited. However, they are not bio-based nor from natural and industrial side-streams [25–27,29,30] and their production and exploitation can be dangerous [24].

Therefore, in the last few years, more widespread attention has been focused on eco-friendly and bio-based adhesion promoters. Within this framework, the interest in natural polyphenolic compounds is rising [31,32], since they show key benefits, such as non-toxicity, biodegradability, ease of extraction from natural sources and agro-food waste, availability, low cost, and high affinity for metallic surfaces [33–36]. Polyphenols include various ubiquitous molecules, like tannins, and their characteristic catechol groups can interact with many kinds of surfaces and, particularly with steel thanks to their action as polydentate ligands for metal ions [33,37–42]. The coordinate interactions between tannins and iron ions have been extensively studied and produce black mono and bis-complexes, denominated iron tannates [33,40]. The coating adhesion enhancement by natural tannins, including tannic acid (Fig. 1b), on steel substrates was investigated [33,41–50]. Wang et al. achieved a highly performed tannic acid-based additive as an adhesion promoter for a UV-curable coating for low-carbon steel. As the tannins hydrophilic nature makes them usually not compatible with most organic resins, they synthesized acrylated tannic acid with glycidyl methacrylate, which is harmful and corrosive. Moreover, the resin used was a standard bisphenol A epoxy acrylate [50].

Lastly, surface oxides, commonly named “scale” [51], and other contaminants on the steel surface can affect coating adhesion. Hence, their removal is crucial to recover a clean, bare, and smooth steel

surface. One of the most common industrial methods is a pickling process in either sulfuric acid or hydrochloric acid aqueous baths [51–53]. However, the extensive use of acids proves not sustainable and implies several hazards, which can be avoided by plasma treatment. Plasma treatment is highly efficient, energy-saving, easily controlled, and environmentally friendly and it can be utilized as a technology for steel surface engineering [54], a decontamination method in the food industry [55] and a technique for improving coatings adhesion [56,57].

With the aim to obtain a sustainable coating with strong adhesion properties on low-carbon steels, through the eco-friendly technique of UV-curing, the current study proposes tannic acid (TA), extracted from natural sources, as a bio-based and chemically unmodified additive for the UV-curable epoxidized soybean oil-based (ESO) coating. We examined the cationic photopolymerization of coatings formulations with different weight ratios of ESO/TA by real-time FTIR spectroscopy and photo-DSC analysis. The thermo-mechanical and surface properties of the UV-cured coatings, with and without the tannic additive, were deeply assessed, as well as the TA effect on adhesion by the cross-cut tape test. Finally, this study also provided an investigation of the effects of pickling and plasma steel pre-treatments on the coatings' adhesion.

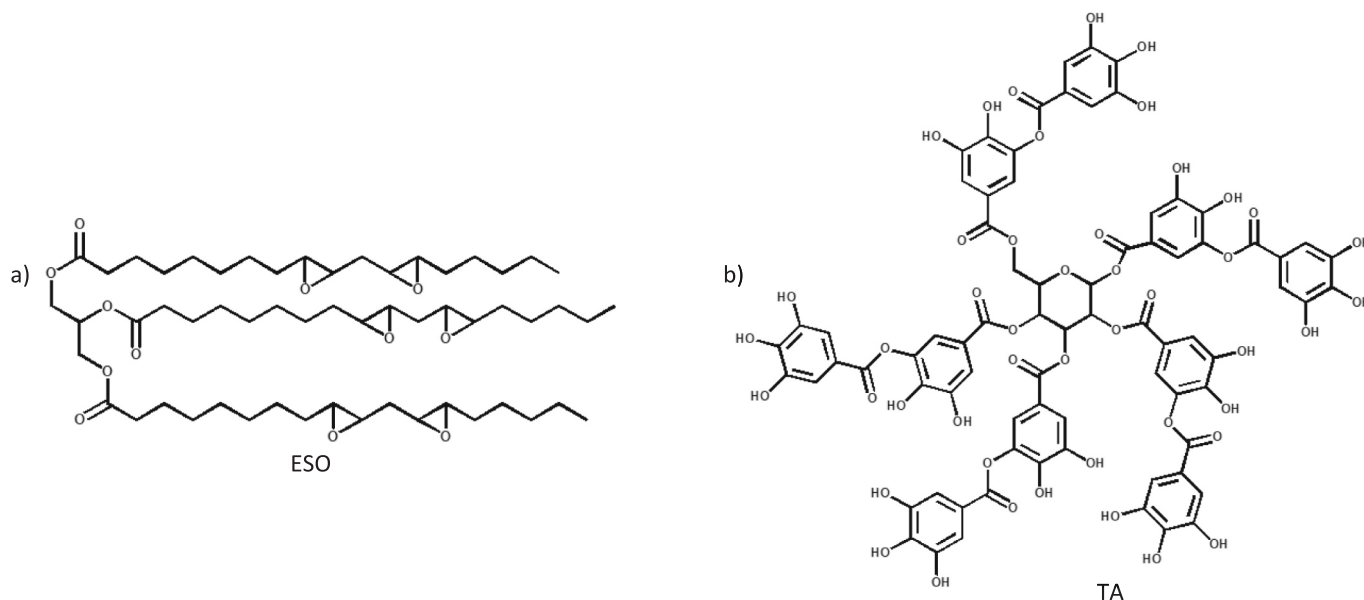
## 2. Materials and methods

### 2.1. Materials

The extract of tara Tan'Active T80 (TA) from *Caesalpinia spinosa* was supplied by Silvateam S.p.A. (San Michele Mondovì, Cuneo, Italy) and it is composed of 100 % gallic tannins with a tannic acid content >90 %. The epoxidized soybean oil (ESO) was synthesized and provided by HOBUM Oleochemicals GmbH (Hamburg, Germany). The composition

**Table 1**  
Composition of epoxidized soybean oil (ESO).

Oxirane content [%]	Acid value [mg KOH/g]	Viscosity at 20 °C [mPa*s]	Iodine value [g I <sub>2</sub> /100 g]	Color [Gardner]	Biobased carbon content [%]
6.5–7.5	Max. 0.5	400–600	Max. 3.5	Max. 2	100



**Fig. 1.** Chemical structures of a) epoxidized soybean oil (ESO) and b) tannic acid (TA).

of the vegetable oil is provided in Table 1.

The cationic photoinitiator (triarylsulfonium hexafluoroantimonate salt), mixed 50 wt% in propylene carbonate, was purchased from Sigma-Aldrich, as well as propylene carbonate (PC, ReagentPlus®, 99 %) acetone (ACS reagent, 99.5 %) and hydrochloric acid (ACS reagent, 37 %). The measuring liquid for the contact angle analysis was Water (ROMIL-SpS™ Super Purity Solvents) from ROMIL.

To characterize the adhesion performances of the coatings, Q-PANEL® standard test substrates (ASTM A1008, low-carbon steel, 0.51 mm thick, Q-Lab) were used and cut into 10 mm × 10 mm pieces. The chemical composition of these materials is (wt%): <0.15 C, <0.60 Mn, <0.03 P, <0.035 S, and balance Fe.

## 2.2. Preparation of formulations

The different formulations were prepared as follows. After pouring around 0.5 g of ESO into a vial, 2 parts per hundred resin (phr) of the photoinitiator was added [13,58]. Then, the vial was covered in an aluminum foil to prevent light exposition and the formulation was mechanically stirred for a few minutes.

Since the pristine extract of tara Tan'Active T80 (TA) is not soluble in ESO matrix, TA solutions of 30 wt% or 40 wt% in propylene carbonate were prepared by sonication at room temperature until completely solubilized. Propylene carbonate was chosen as it is the same solvent as the photoinitiator. The described above method was used to prepare ESO-based formulations containing TA, by adding a specified amount of TA solution to obtain a definite weight ratio of ESO to TA. Table 2 summarizes the different formulations.

## 2.3. Pre-treatment of the steel surface

To assess the coating adhesion properties, the surface of low-carbon steel substrates (Q-PANEL®) was pre-treated before the coating deposition to remove any impurities, such as carbon contaminants or rust formed during the steel's storage, and thus to improve steel surface reactivity [52,56,57,59,60]. Firstly, steel samples were degreased by sonification in acetone for 5 min at room temperature and then dried with compressed air. Hereafter, the steel samples were divided into two sets.

A part of the samples underwent the pickling process in 2 M HCl for 5 min. Subsequently, they were rinsed with distilled water and dried with compressed air.

The surfaces of the second set were treated with an air plasma (Tucano, Gambetti Kenologia Srl, Italy) for 10 min at 100 W and quickly packed with an aluminum foil after the process to prevent further contamination.

All steel substrates were immediately coated by the various formulations (Table 2) after the surface pre-treatment.

## 2.4. Photopolymerization of coatings

The formulations were deposited on the pre-treated steel substrates with a film bar, to ensure a thickness of 100 µm. The photocrosslinking

process was carried out at room temperature for 90 s by using Dymax ECE 5000 with a light intensity of 130 mW/cm<sup>2</sup>. The UV lamp's emission ranged from 275 to 500 nm with a maximum intensity at 365 nm.

## 2.5. Characterization of the formulations

### 2.5.1. UV–Vis spectroscopy

The UV–Vis spectrophotometer (UV-2600, Shimadzu, Japan) was exploited to assess the absorption competition in the UV region of the photoinitiator and TA. For the analysis, a 2 wt% TA solution in propylene carbonate and a 15 wt% photoinitiator solution in propylene carbonate were produced, while pure propylene carbonate was used as blank.

### 2.5.2. Fourier transform infrared spectroscopy (FTIR)

The Fourier Transform Infrared spectroscopy (FTIR) analyses were conducted using a Thermo Scientific Nicolet iS50 FTIR spectrometer (Thermo Fisher Scientific, Milano, Italy). The spectra were recorded in the range of 4000–600 cm<sup>−1</sup> as 32 scans with a spectral resolution of 4.0 cm<sup>−1</sup>.

To evaluate the composition of the formulations, the FTIR instrument equipped with a diamond crystal ATR accessory was used.

The photocrosslinking process was monitored by real-time FTIR in transmission mode in the air at room temperature. The photocurable liquid formulations were spread with an average film thickness of about 12 µm on a silicon wafer by a film bar. The conversion degree was assessed by the disappearance of the double epoxy peaks centered at 846 cm<sup>−1</sup> and 823 cm<sup>−1</sup> [23,61,62]. The peak at 1744 cm<sup>−1</sup>, assigned to the C=O stretching of ESO, was assumed to be unaffected by UV irradiation [14,63] and thus it was taken as the reference. The conversion degree during the exposure time was calculated according to Eq. (1).

$$\text{Conversion [\%]} = \frac{\left( \frac{A_{\text{epoxy}}}{A_{\text{ref}}} \right)_{t=0} - \left( \frac{A_{\text{epoxy}}}{A_{\text{ref}}} \right)_t}{\left( \frac{A_{\text{epoxy}}}{A_{\text{ref}}} \right)_{t=0}} \times 100 \quad (1)$$

where  $A_{\text{epoxy}}$  and  $A_{\text{ref}}$  are the areas of the epoxy ring peak and the reference peak, respectively, evaluated at different times.

All measurements were repeated three times, and the data were recorded and analyzed by using the Thermo Fischer Scientific Omnic software.

### 2.5.3. Differential scanning photo calorimetry (photo-DSC)

The differential scanning photo calorimetric (photo-DSC) analyses were performed on a Mettler Toledo DSC instrument equipped with Gas Controller GC100. The DSC was supplied with a mercury lamp (Hamamatsu Lightnigcure™ LC8, Hamamatsu Photonics) with an optical fiber to directly irradiate the sample. The UV light emission was centered at 365 nm with an intensity of 100 mW/cm<sup>2</sup>. The photocurable samples (8–13 mg) were poured into an open 40 µL aluminum pan, whereas an empty pan was used as a reference. The experiments were performed at room temperature (25 °C) under inert in a nitrogen atmosphere (N<sub>2</sub> flow rate of 40 mL/min). The samples were irradiated two times for 5 min. The second irradiation step was useful to verify the complete curing and create the baseline. The curing curve was obtained by subtracting the second curve from the first. All experiments were carried out in triplicate and the data were processed by Mettler Toledo STARE software V9.2.

### 2.5.4. Dynamic mechanical thermal analysis (DMTA)

Dynamic thermal-mechanical analysis was carried out with a Triton Technology device (Tritec 2000 DMA). The samples were UV-cured in a silicon mold with dimensions of 17 mm × 8 mm × 1 mm. The initial temperature (−50 °C) was achieved by cooling the test chamber with liquid nitrogen. The measurements were run by applying uniaxial tensile

**Table 2**  
Formulations used in this study.

Formulation	ESO/TA [weight ratio]	TA solution added [wt%]	TA content [wt%]	PC content [wt%]	Photoinitiator content [wt%]
ESO/0TA	100/0	–	–	–	2
ESO/3TA	90/10	30	3	7	2
ESO/4TA	90/10	40	4	6	2
ESO/6TA	80/20	30	6	14	2
ESO/8TA	80/20	40	8	12	2
ESO/9TA	70/30	30	9	21	2

stress at the frequency of 1 Hz with a heating rate of 5 °C/min and were concluded when the rubbery plateau was reached. The storage modulus ( $E'$ ) and the loss factor ( $\tan\delta$ ) were recorded as a function of temperature.

Glass transition temperature ( $T_g$ ) was detected as a maximum of the  $\tan\delta$  curve. The ratio between the dissipative modulus ( $E''$ ) and the storage modulus ( $E'$ ) corresponds to the  $\tan\delta$  and the maximum of the  $\tan\delta$  can be attributed to  $T_g$ . Moreover, the crosslinking density ( $\nu_c$ ) was estimated by using an equation derived from the statistical theory of rubber elasticity (Eq. (2)). As this equation approximates the system, it was used only to qualitatively compare the level of crosslinking among the obtained networks [61].

$$\nu_c = \frac{E'_R}{3RT} \quad (2)$$

where  $\nu_c$  is the number of moles of network chains per unit volume of the crosslinked network,  $E'_R$  is the storage modulus values in the rubbery plateau region extracted from the graph at 50 °C above  $T_g$ ,  $R$  is the gas constant and  $T$  is the absolute temperature (i.e., at  $T_g + 50$  °C). The test was repeated three times for each type of formulation.

## 2.6. Characterization of the coatings

To evaluate the coating properties, the formulations were photopolymerized on the pre-treated steel substrates, as described above.

### 2.6.1. Contact angle

The contact angle tests were carried out with a drop shape analyzer (DSA100, Krüss) equipped with a video camera. The analyses were conducted at room temperature through the sessile drop technique placing the water droplet (5  $\mu$ l) on a free surface film. Three to six measurements were performed on each sample and the values were averaged.

### 2.6.2. Pencil hardness and Leeb rebound hardness tests

The hardness of the coatings was assessed through two different tests. The pencil hardness was determined according to the ASTM D3363 standard [64]. Several pencils ranging from 6B to 4H were employed. The final pencil (in order of hardness) that did not leave a scratch on the film surface was used to attribute the hardness value. Moreover, the Sauter HMO mobile Leeb Hardness Tester was used to evaluate the coatings' hardness by following the ASTM A956/A956M standard [65]. Four measurements were taken for each type of sample to have an average value.

### 2.6.3. Adhesion tests

To assess the coatings' resistance to separation from the steel substrates, the adhesion test was carried out according to the BS EN ISO 2409:2020 standard [66]. The Elcometer 107 Cross Hatch Cutter was used to evaluate the adhesion of the photocrosslinked coatings on the steel substrates. The insert number 3 was used as a cutter to perform the test. The cut areas were carefully visually examined with a viewing lens and were classified according to Table 3, using the images as a guide. After the adhesion test, the steel samples were observed by optical microscope (Reichert-Jung MeF3, Leica-Microsystems Srl).

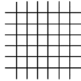
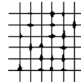
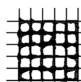

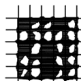
## 3. Results and discussion

### 3.1. Investigation on cationic photopolymerization

Fig. 2 shows the FTIR spectra of ESO/OTA and ESO/9TA compared to the ones of the raw materials (ESO and TA). The ESO spectrum is characterized by narrow peaks at 2927  $\text{cm}^{-1}$  and 2855  $\text{cm}^{-1}$  which were assigned to the  $-\text{CH}_2-$  asymmetrical and symmetrical stretching vibration, respectively. The signal with high intensity at 1744  $\text{cm}^{-1}$  was

**Table 3**

Classification of test results in accordance with BS EN ISO 2409:2020 standard.

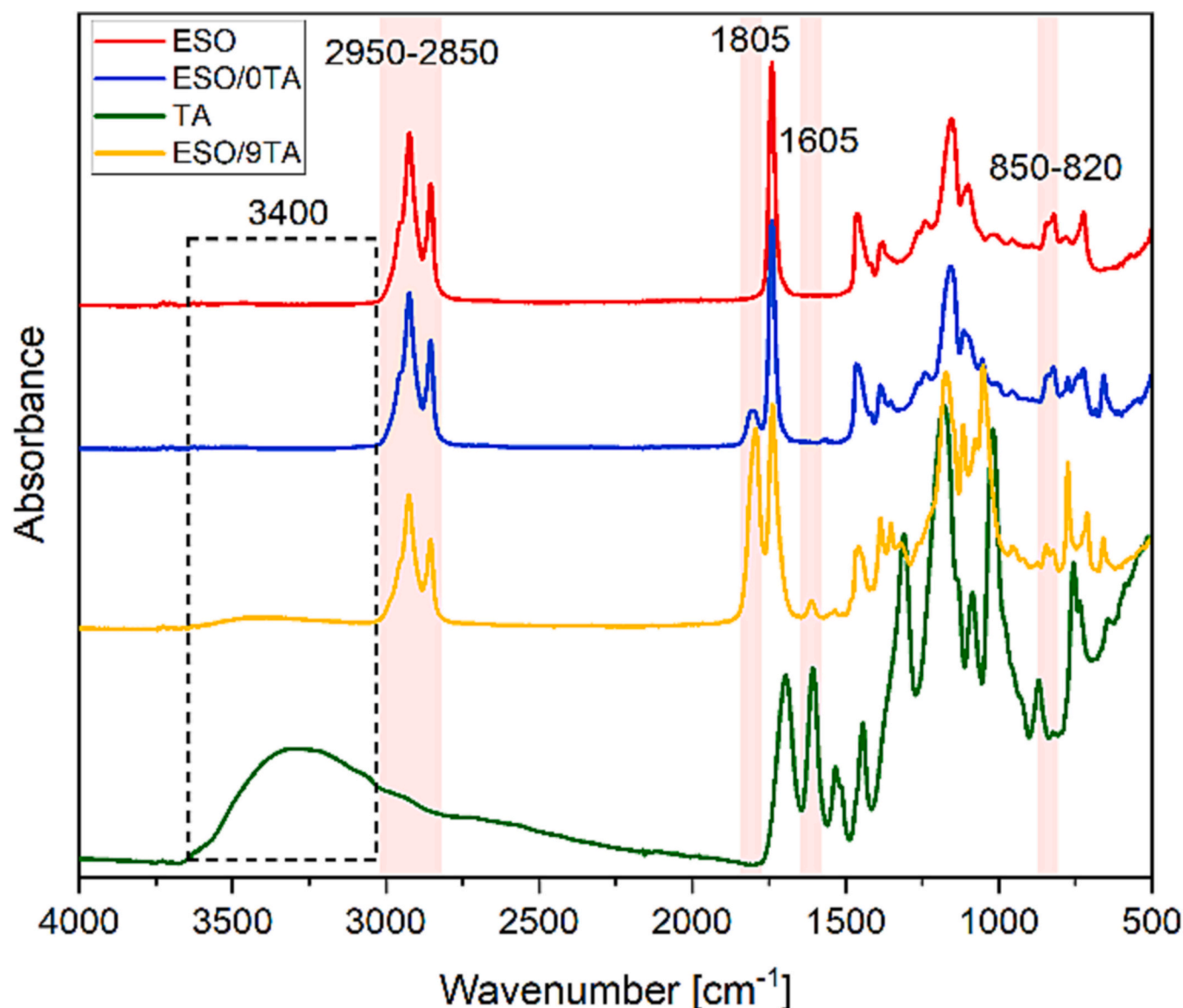
Classification	Description	The appearance of cross-cut areas from which flaking has occurred <sup>a</sup>
0	The edges of the cuts are completely smooth; none of the squares of the lattice is detached.	
1	Detachment of small flakes of the coating at the intersections of the cuts. A cross-cut area lower than 5 % is affected.	
2	The coating has flaked along the edges and/or at the intersections of the cuts. A cross-cut area >5 %, but lower than 15 %, is affected.	
3	The coating has flaked along the edges of the cuts partly or wholly in large ribbons, and/or it has flaked partly or wholly on different parts of the squares. A cross-cut area >15 %, but lower than 35 %, is affected.	
4	The coating has flaked along the edges of the cuts in large ribbons and/or some squares have detached partly or wholly. A cross-cut area >35 %, but lower than 65 %, is affected.	
5	Any degree of flaking that cannot even be classified by classification 4	—

<sup>a</sup> The figures are examples of a cross-cut within each step of the classification. The percentages stated are based on the visual impression given by the pictures and the same percentages will not necessarily be reproduced with digital imaging.

generated by the stretching vibration of ESO's ester  $\text{C}=\text{O}$  groups and the peaks at about 846  $\text{cm}^{-1}$  and 823  $\text{cm}^{-1}$  were attributed to stretching and bending vibrations of the  $\text{C}-\text{O}-\text{C}$  of the epoxy rings, respectively. These characteristic signals of ESO were present also in the spectra of the photocurable formulations, as can be seen from the ESO/OTA and ESO/9TA spectra reported in Fig. 2. Moreover, the spectra of ESO/OTA and ESO/9TA show a new peak at 1805  $\text{cm}^{-1}$  assigned to the carbonyl group of PC, which is the solvent of both photoinitiator and TA solutions. The higher intensity of this peak in the spectrum of ESO/9TA was due to the higher amount of solvent from the addition of the TA solution to the ESO formulation.

The photopolymerization kinetics of ESO-based formulations with and without TA was followed by real-time FTIR (Fig. 3a). Once the light was turned on, the intensities of these peaks started to decrease as a consequence of the epoxy ring opening [13,61,67,68]. Simultaneously, the broad band at around 3400  $\text{cm}^{-1}$  appeared and its intensity increased during the irradiation time. This demonstrated that the formation of  $-\text{OH}$  groups was caused by the ring-opening polymerization reaction [61,68]. The mechanism of this light-induced polymerization reaction is schematically shown in Fig. 3b. Briefly, the cationic photoinitiator (triarylsulfonium hexafluoroantimonate salt) produces a Brønsted acid upon UV irradiation. The presence of the photogenerated protonic acid promoted the ring-opening polymerization of epoxides [13]. The complete conversion was achieved after 90 s of UV irradiation and the average percentages of conversion are reported in Table 4. As shown in Fig. 4, the TA addition to the ESO formulation significantly increased the photocuring reactivity. After 30 s of UV exposure, the conversion reached for the formulation ESO/OTA was around 55 %, while with the addition of TA, the conversion degree was about 20 or 25





**Fig. 2.** ATR-FTIR spectra of epoxidized soybean oil (ESO, red line), ESO formulation without tannin additive (ESO/0TA, blue line), tannic acid (TA green line), and ESO formulation with tannin additive (ESO/9TA, yellow line). (For interpretation of the references to color in this figure legend, the reader is referred to the web version of this article.)

% higher. After just 60 s, the conversion of the resins with TA reached around 90 %, unlike ESO/0TA. Lastly, a complete conversion for the formulations with TA was achieved after 90 s of irradiation, whereas ESO/0TA showed a conversion degree of only about 72 %. The different formulations with TA showed very similar conversion degrees, considering the standard deviations.

Photo-DSC analysis was performed on the same formulations to corroborate the real-time FTIR data. The different resins were tested in the same temperature curing conditions, i.e., 25 °C. This investigation revealed some critical parameters, including the time at which the maximum rate of heat evolution was reached ( $t_{\text{peak}}$ ), the height of the exothermic peaks ( $h_{\text{peak}}$ ), and the heat release ( $\Delta H$ ), estimated as the total enthalpy from the curing peak integration (Table 3). In Fig. 5a, the photo-DSC thermograms are collected. As can be noticed, the addition of TA to the photocurable formulations significantly increased  $\Delta H$  values. These results can be explained by the chain-transfer mechanism, known as the activated monomer mechanism (Fig. 5b). During the propagation step, the epoxy ion undergoes nucleophilic attack by the polyphenol generating a protonated ether. The charge of this compound is

neutralized by another epoxy group and the growth of the polymeric chain is concluded. As a consequence, this process regenerates a hydroxide terminal that propagates the termination and the chain-transfer processes. The overall effect consists of an acceleration of the epoxy ring conversion and thus, of the crosslinking and a reduction of crosslinking density [18,69–72].

The  $h_{\text{peak}}$  was proven to be proportional to the polymerization rate and hence it confirmed the beneficial effect of tannins on the crosslinking kinetic. Indeed, as previously observed from the curves in Fig. 4, the TA addition into ESO matrix significantly increased the  $h_{\text{peak}}$  values and thus the photopolymerizations of coatings with the tannic additive were faster than ESO/0TA. As a last consideration, the time at the maximum rate of polymerization ( $t_{\text{peak}}$ ) increased as the TA concentration and amount increased. This result can be clarified by the absorption competition between TA and the photoinitiator, which determines a delay in crosslinking kinetics of formulations with TA compared to pristine ESO. Indeed, as Fig. 6 displays, TA and the photoinitiator absorb in the same wavelength range with  $\lambda_{\text{max}}$  at around 315 nm and 353 nm, respectively. Therefore, the presence of the

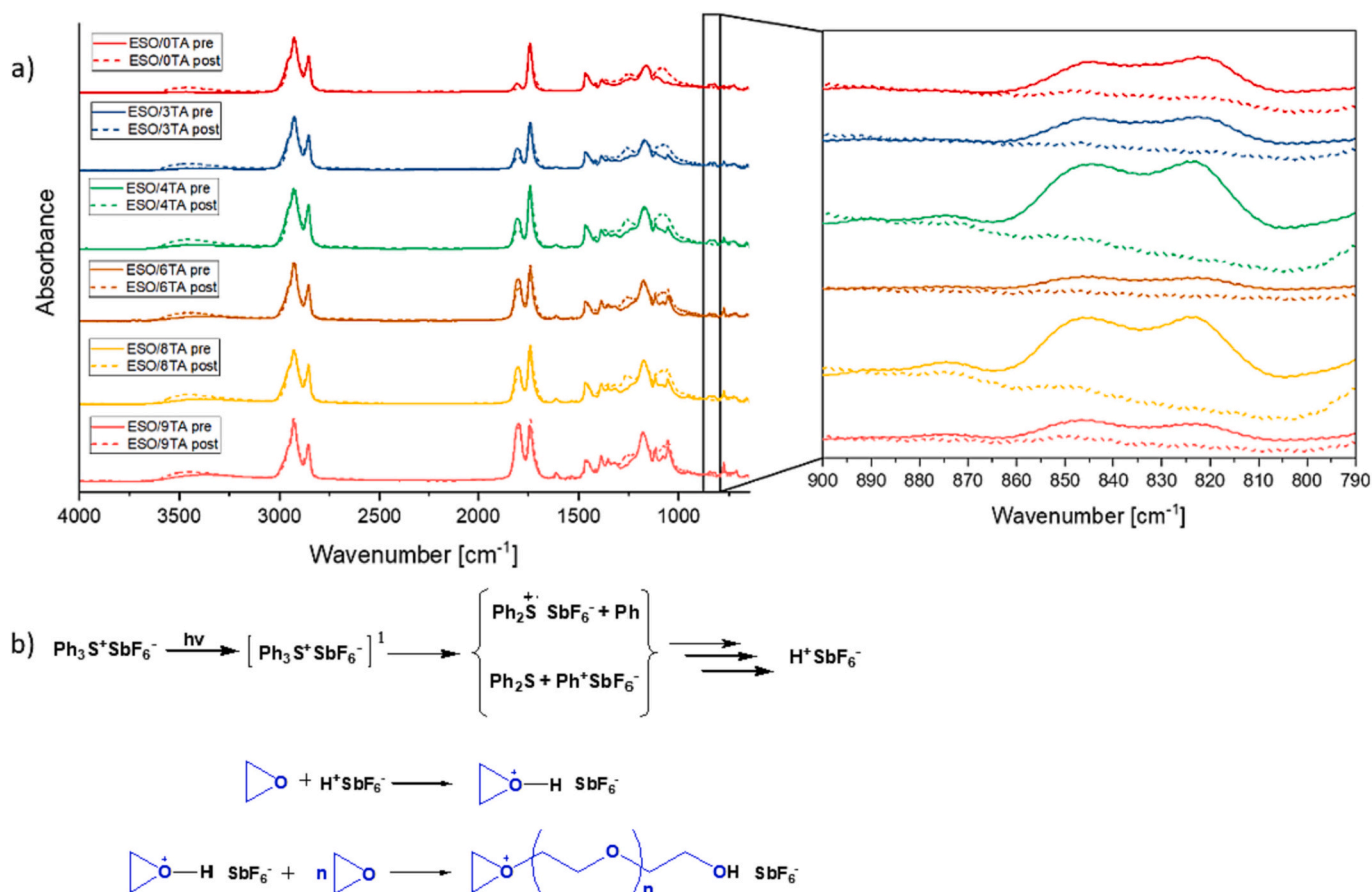


Fig. 3. a) FTIR spectra recorded before (–pre, solid line) and after (–post, dash line) the irradiation; b) schematic representation of the cationic photopolymerization via epoxy-ring opening.

Table 4

Properties of crosslinked resins.

Formulation	Conversion degree <sup>a</sup> [%]	$t_{\text{peak}}$ [s]	$h_{\text{peak}}$ [W/g]	$\Delta H$ [J/g]	$T_g$ [°C]	$E'$ [kPa]	$\nu_c^b$ [mol/cm <sup>3</sup> ]
ESO/0TA	72 ± 2	10.3 ± 4.4	5.6 ± 1.2	171.7 ± 21.3	13 ± 3	14,428 ± 1698	1720 ± 190
ESO/3TA	87 ± 1	13.3 ± 0.5	9.8 ± 1.2	332.0 ± 13.0	5 ± 3	3791 ± 417	462 ± 47
ESO/4TA	93 ± 2	17.2 ± 0.9	8.1 ± 0.5	312.1 ± 5.9	7 ± 2	4272 ± 62	519 ± 10
ESO/6TA	87 ± 1	16.1 ± 1.0	7.2 ± 3.2	279.6 ± 49.5	2 ± 1	1709 ± 165	215 ± 25
ESO/8TA	94 ± 4	20.7 ± 0.6	5.4 ± 0.6	253.9 ± 21.9	4 ± 1	1779 ± 95	217 ± 12
ESO/9TA	88 ± 2	17.0 ± 2.3	4.5 ± 0.2	195.3 ± 1.2	–5 ± 2	877 ± 110	114 ± 8

<sup>a</sup> Estimated after 90 s of UV irradiation according to Eq. (1).

<sup>b</sup> Calculated by Eq. (2).

polyphenolic compound determined, on one side, the enhancement of the cationic photopolymerization rate, but, on the other side, a delay in the initiation step. Moreover, although the amount of solvent in the coating system is low (Table 2),  $t_{\text{peak}}$  values can be also affected by the solvent content added in the formulation. An antagonistic effect occurred, since the  $t_{\text{peak}}$  decreased as the PC content increased. The higher PC amount in the formulation caused a viscosity reduction. Consequently, in a less viscous formulation, the chains had greater mobility and were more easily able to interact with the photoinitiator. goole.

Considering all the kinetic parameters assessed, TA concentration in the coating system increase corresponded with an increase in the number of OH groups, that could participate in the activated monomer mechanism. This explained the higher conversion degree of ESO/4TA and ESO/8TA than ESO/3TA and ESO/6TA formulations (Table 4), which were prepared with the 30 wt% TA solution and had the same

ESO/TA weight ratios, respectively (Table 2). The photo-DSC analysis highlighted kinetic parameters of the formulations prepared with the same weight ratio but with different concentrations of the TA solution (ESO/3TA and ESO/4TA, ESO/6TA and ESO/8TA) comparable to each other, taking into account the standard deviations. However, the increase in TA content in ESO/4TA, ESO/8TA and ESO/9TA formulations also implies greater absorption competition between TA and the photoinitiator resulting in an increase in  $t_{\text{peak}}$ . Despite containing the highest TA content, ESO/9TA showed a lower  $t_{\text{peak}}$  than ESO/4TA and ESO/8TA formulations due to the higher PC content, which facilitated the interaction between the monomer and the photoinitiator. Therefore, as can be outlined from the kinetic parameters in the Table 4, ESO/3TA and ESO/4TA formulations showed higher values in the conversion degree, the polymerization rate, and the total enthalpy with minimum delays.

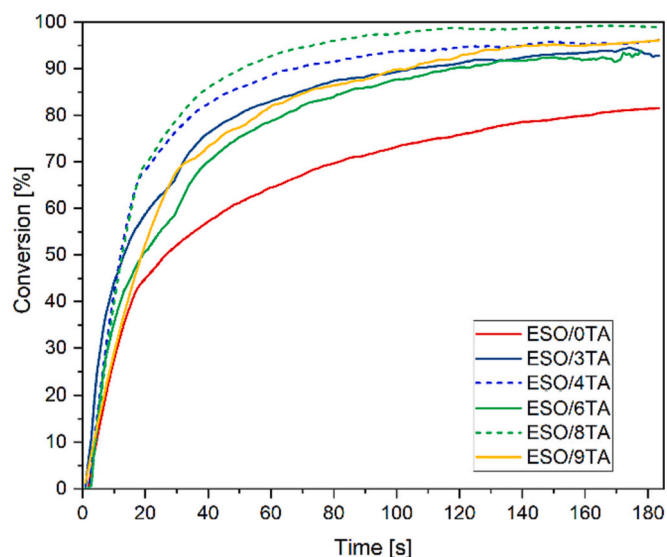


Fig. 4. Conversion of epoxy group as a function of time from real-time FTIR analysis of ESO/TA formulations changing the weight ratio of ESO/TA.

### 3.2. Thermal and viscoelastic properties

Formulations based on ESO were UV-cured and analyzed by DMTA to thoroughly characterize their thermal and viscoelastic properties. Indeed, through this technique, the storage ( $E'$ ) and dissipative ( $E''$ ) moduli of the materials can be evaluated in a large temperature range as well as the glass transition temperature ( $T_g$ ), corresponding to the maximum of  $\tan\delta$ . The registered  $\tan\delta$  curves of the UV-cured films are reported in Fig. 7a. By increasing the TA content in the resin,  $T_g$  decreased with a shift of the maximum of  $\tan\delta$  curves toward a lower temperature, ranging from 13 to  $-5^\circ\text{C}$  (Table 4). According to the values outlined in Table 4, the crosslinking density ( $\nu_c$ ) decreased by increasing TA and hence PC amounts. As affirmed above, the activated monomer mechanism, which involves the multiple phenols of TA, causes a reduction of the crosslinking density due to the chain transfers and implies an increase in the mobility of polymeric chains, which is reflected by lower  $T_g$  values. Furthermore, the broader and flatter  $\tan\delta$  curve of 100 ESO suggested a more heterogeneous network with a wider distribution of chain relaxation [73].

### 3.3. Surface properties

The surface properties of the UV-cured ESO and ESO/TA coatings on

low-carbon steel substrates were investigated by contact angle and two types of hardness tests (pencil hardness and Leeb rebound hardness).

The water contact angle values for all formulations are very similar to each other (Table 5). No decrease in the coating hydrophobicity was recorded with the addition of a high number of phenols to ESO-based resins. Hence, the tannin additive, which is hydrophilic per se, was present in the coating bulk and had no effect on the UV-cured film wettability. This is of relevance because the hydrophobicity of the coatings is required for protective and anti-corrosion actions.

Concerning the coatings' hardness, as shown in Table 4, the correlation between  $\nu_c$  and the final properties of the coatings is evident. The addition of TA solution to the ESO formulation decreased the surface hardness of the coatings, since the crosslinking reduction achieved by the TA addition diminished the rigidity of the network, as detected by  $T_g$  values.

### 3.4. Adhesion performances

The ability to firmly adhere to the substrate is a crucial property of a coating. Therefore, adhesion tests were performed on the differently pre-treated and coated steel samples. The pre-treatment effect on the interaction between the coating and steel surface and the potential application of TA as an adhesion promoter were assessed. Table 5 collects the adhesion data of UV-cured coatings on the pickled or plasma-treated steel substrates evaluated according to the BS EN ISO 2409:2020 classification. Within this empirical method, the capacity of coatings to remain adherent to the substrates is visually assessed and divided into 5 classes based on the percentage of coating affected by the detachment (Table 3).

It can be noted that the ESO/0TA coating proved a very inadequate adhesion on the steel surface (with a value of 4 and 5, respectively, for the pickling and plasma pre-treated surface). Moreover, as shown in the optical microscope images of the samples after the adhesion test (Figs. 8 and 9), the ESO/0TA coating was completely removed from the plasma pre-treated steel (Figs. 8a and 9a). ESO/0TA on the pickled steel (Fig. 8a) flaked only along the edges of the cuts while some squares detached partially or wholly. However, the addition of TA to the ESO-based coating outstandingly enhanced the adhesion property probably due to the tannin's ability to coordinate iron ions (Fig. 10). Indeed, for all samples regardless of the pre-treatment, the coating adhesion significantly improved as the added TA amount increased. Therefore, as depicted in Fig. 10, TA could act as a "bridge" between the steel surface and the ESO coating. In detail, the ESO/TA coatings showed the best adhesion properties on the pickled steel (Fig. 8), where a cross-cut area lower than 5 % was affected and the edges of the cut were completely smooth. Concerning the coated plasma-treated samples, the ESO/3TA

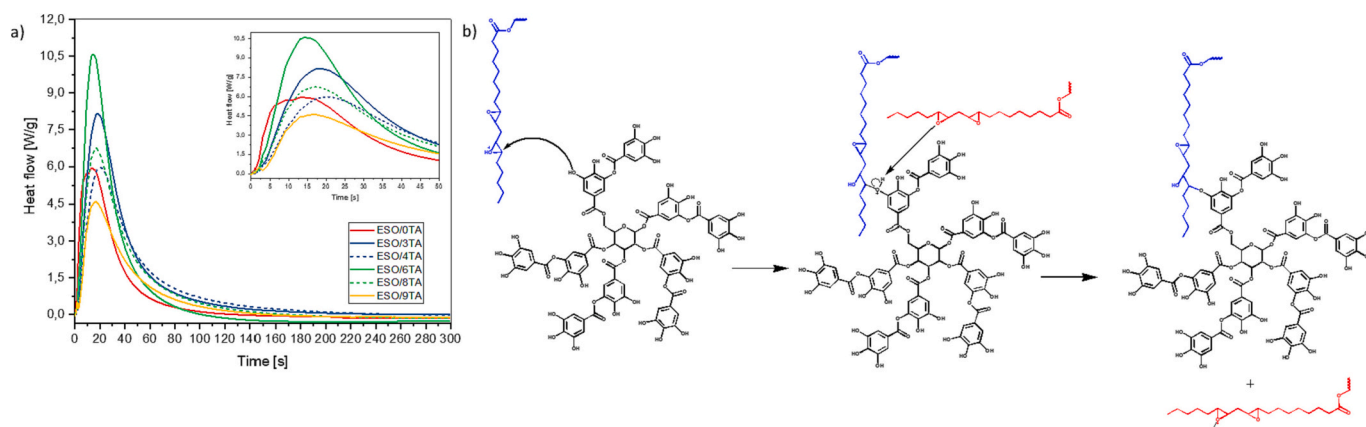
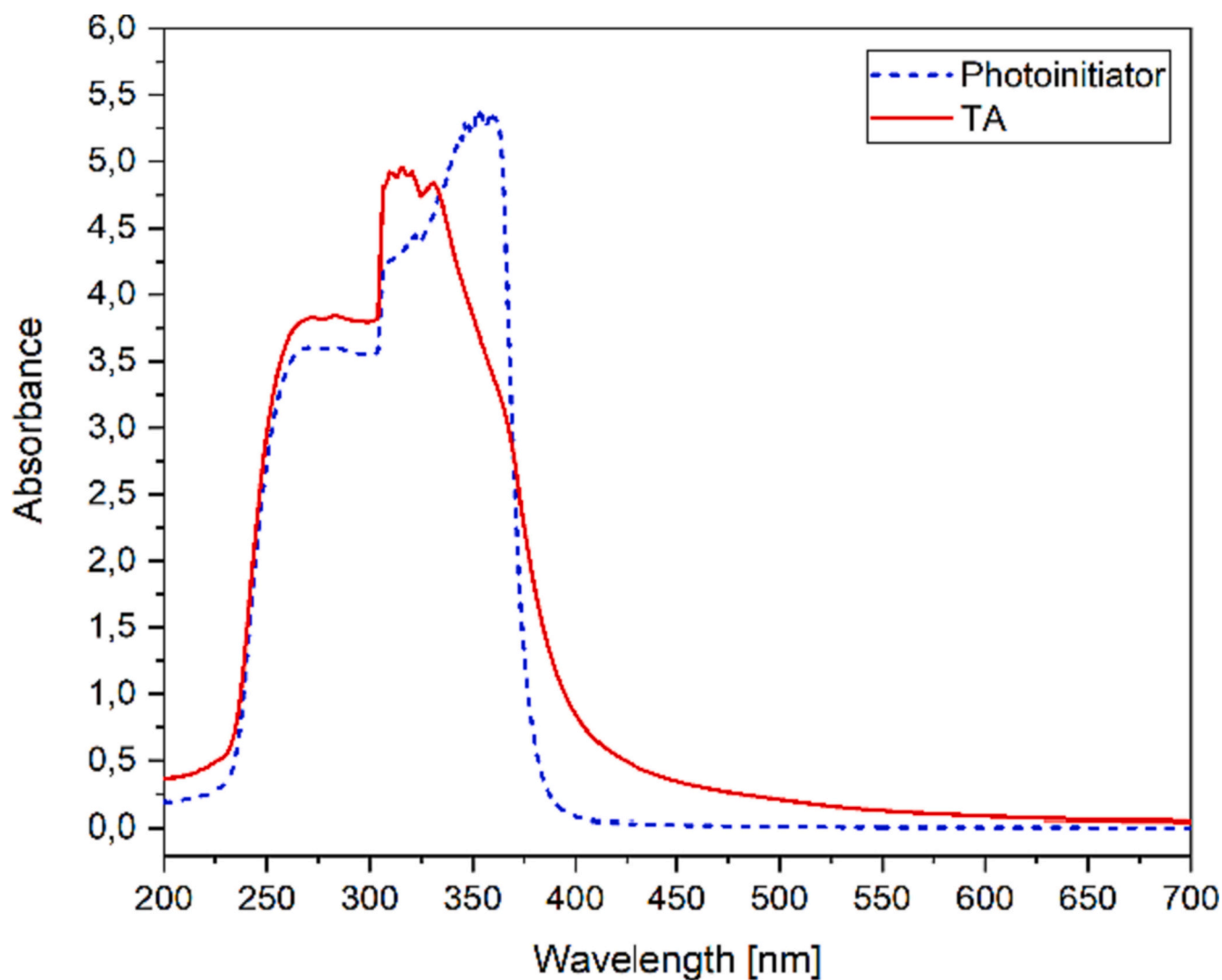
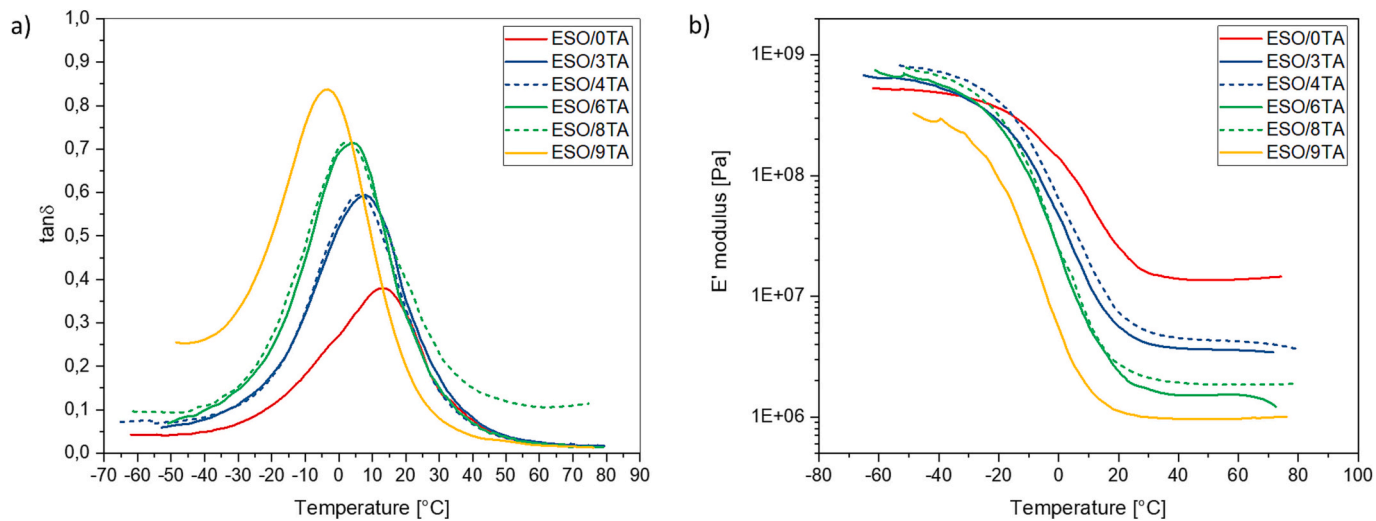


Fig. 5. a) Photo-DSC thermograms for ESO/TA formulations with different ESO/TA weight ratios; b) scheme of the activated monomer mechanism, which involves ESO and TA.





**Fig. 6.** UV-Vis spectra of photoinitiator (blue dash line) and TA (red solid line). (For interpretation of the references to color in this figure legend, the reader is referred to the web version of this article.)



**Fig. 7.** a)  $\tan\delta$  curves and b) storage ( $E'$ ) modulus curves from DMTA analysis on the UV-cured ESO/TA formulations with different ESO/TA weight ratios.

**Table 5**  
Surface properties and adhesion performances of UV-cured coatings.

Formulation	Contact angle [°]	Pencil hardness	Leeb hardness	Adhesion test – pickling pre-treatment <sup>a</sup>	Adhesion test – plasma pre-treatment <sup>a</sup>
ESO/0TA	85.4 ± 0.7	4H	324 ± 93	4	5
ESO/3TA	84.7 ± 2.4	3H	288 ± 58	1	2
ESO/4TA	85.2 ± 0.4	F	248 ± 55	0	2
ESO/6TA	85.9 ± 2.7	H	242 ± 65	0	1
ESO/8TA	86.1 ± 0.8	F	213 ± 36	0	1
ESO/9TA	86.1 ± 0.3	HB	200 ± 45	0	1

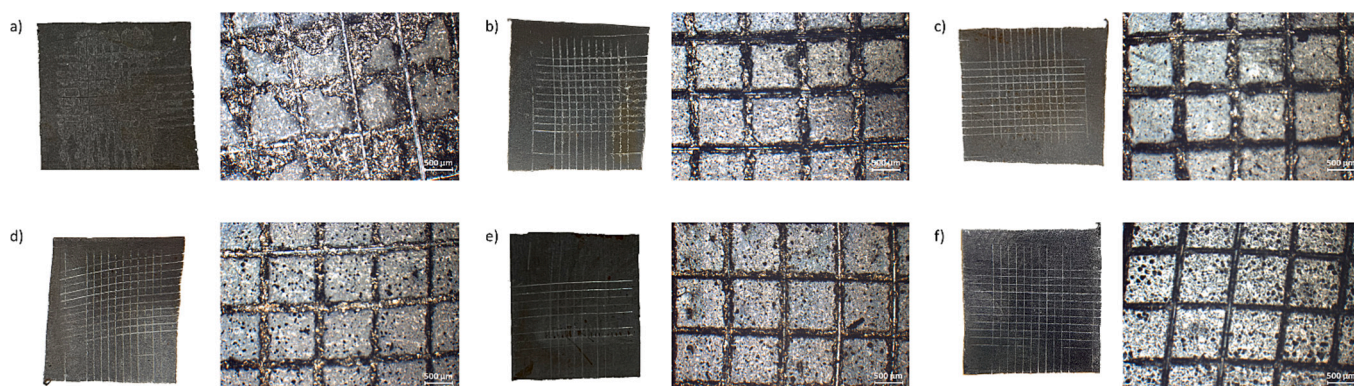
<sup>a</sup> Classification according to BS EN ISO 2409:2020 standard.

and ESO/4TA coatings flaked along the edges and cut intersections, affecting a cross-cut area >5 % but lower than 15 %, as observed in Fig. 9b-c. Instead, thanks to the TA increase in the coatings (ESO/6TA, ESO/8TA, and ESO/9TA), the detachment of small flakes at the cut intersections occurred on the plasma-treated samples with a cross-cut area lower than 5 % (Fig. 9d-f).

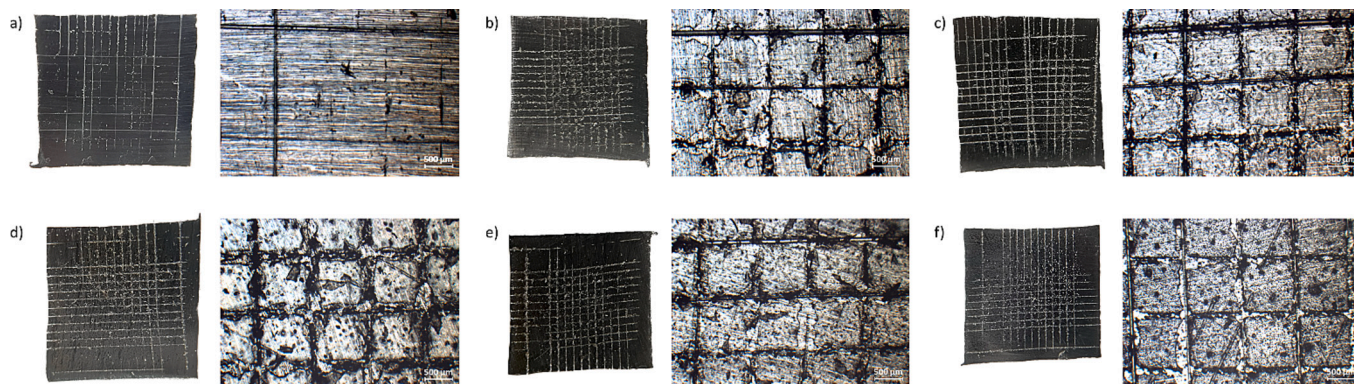
Therefore, the metallic surface pre-treatment, together with the TA presence, affected the coating adhesion. The pickled surface was more reactive and allowed a stronger interaction with the coating, but the good results obtained with a physical and environmentally friendly technique, such as plasma, are of great interest.

#### 4. Conclusions

The present study investigated tannic acid (TA) as an additive in UV-curable coatings based on epoxidized soybean oil (ESO) to promote adhesion on low-carbon steel substrates. Different TA contents were added to the photocurable formulation. The cationic photopolymerization efficiently provided crosslinked networks with a high degree of conversion. In particular, the real-time FTIR and photo-DSC analyses proved that the TA addition to ESO formulations significantly enhanced the conversion thanks to a chain-transfer process, named the activated monomer mechanism, which involves the multiple phenols of TA. However, due to this mechanism, a reduction of the crosslinking density occurred as the TA amount increased. Indeed, the TA presence decreased the thermo-mechanical properties and the hardness of the coatings. Despite that, the very low wettability of coatings was not affected by TA, which was present in the bulk of the coating. Regardless of the type of pre-treatment, an outstanding enhancement of the adhesion of ESO/TA coatings was observed. Furthermore, the effect of the type of steel surface pre-treatment on the ESO/TA coatings adhesion performances was investigated. The best adhesion was found for the pickled steel samples with the TA additive in the coating in different amounts. The adhesion on the steel of coatings with the greater amount of TA, pre-treated with the safer and more environmentally friendly plasma technique than the pickling process, proved particularly enhanced compared to ESO/0TA. The noteworthy adhesion improvement can be attributed to the multiple phenols of TA, that are able to coordinate iron ions and thus act as a “bridge” between the metallic surface and the photocrosslinkable epoxy-based coating. Therefore, this work demonstrates the possibility of achieving sustainable and green photocrosslinked bio-based coatings with enhanced adhesion on steel



**Fig. 8.** Digital photos and optical images (20×) after the adhesion test of pickled steel samples coated by a) ESO/0TA, b) ESO/3TA, c) ESO/4TA, d) ESO/6TA, e) ESO/8TA and f) ESO/9TA.



**Fig. 9.** Digital photos and optical images (20×) after the adhesion test of plasma-treated steel samples coated by a) ESO/0TA, b) ESO/3TA, c) ESO/4TA, d) ESO/6TA, e) ESO/8TA and f) ESO/9TA.



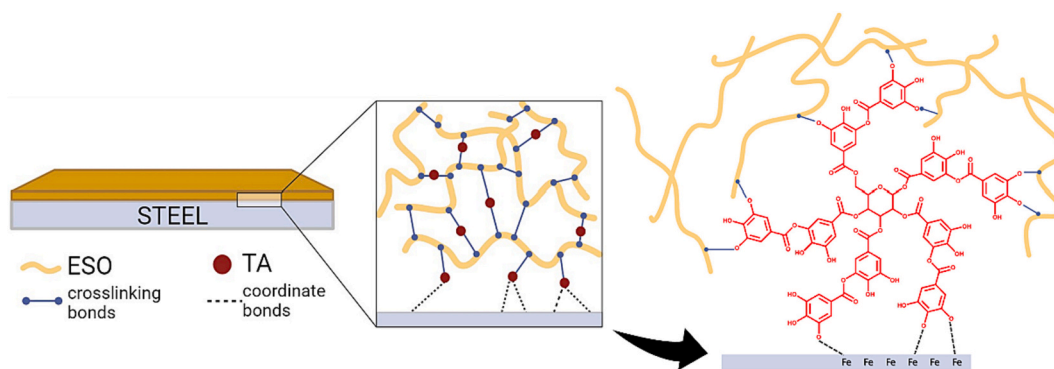


Fig. 10. Scheme of the coating system with TA and representation of the adhesion mechanism between the coating and the steel surface.

thanks to a natural tannic additive. Future outlook may include an optimization of plasma treatment conditions to improve the adhesion efficiency of the bio-based coating and achieve a completely eco-friendly system, that avoids harmful chemicals both in steel pre-treatment and in coating production.

#### CRediT authorship contribution statement

**Rossella Sesia:** Investigation, Formal analysis. **Anna Giulia Cardone:** Formal analysis. **Sara Ferraris:** Data curation. **Silvia Spriano:** Funding acquisition. **Marco Sangermano:** Supervision, Data curation.

#### Declaration of competing interest

The authors declare that they have no known competing financial interests or personal relationships that could have appeared to influence the work reported in this article.

#### Data availability

Data will be made available on request.

#### Acknowledgments

MUR is acknowledged for funding R. Sesia's Ph.D. fellowship (MUR – D.M.1061/2021 – Dottorati di ricerca su tematiche green e dell'innovazione: nuove risorse dal PON Ricerca e Innovazione). Silvateam S.p.A. is acknowledged for the collaboration.

#### References

- [1] R. Auvergne, S. Caillol, G. David, B. Boutevin, J.-P. Pascault, Biobased thermosetting epoxy: present and future, *Chem. Rev.* 114 (2014) 1082–1115, <https://doi.org/10.1021/cr3001274>.
- [2] S. Ma, T. Li, X. Liu, J. Zhu, Research progress on bio-based thermosetting resins, *Polym. Int.* 65 (2016) 164–173, <https://doi.org/10.1002/pi.5027>.
- [3] C. Aouf, J. Lecomte, P. Villeneuve, E. Dubreucq, H. Fulcrand, Chemo-enzymatic functionalization of gallic and vanillic acids: synthesis of bio-based epoxy resins prepolymers, *Green Chem.* 14 (2012) 2328, <https://doi.org/10.1039/C2GC35558B>.
- [4] S. Flint, T. Markle, S. Thompson, E. Wallace, Bisphenol A exposure, effects, and policy: a wildlife perspective, *J. Environ. Manag.* 104 (2012) 19–34, <https://doi.org/10.1016/j.jenvman.2012.03.021>.
- [5] S. Miao, P. Wang, Z. Su, S. Zhang, Vegetable-oil-based polymers as future polymeric biomaterials, *Acta Biomater.* 10 (2014) 1692–1704, <https://doi.org/10.1016/j.actbio.2013.08.040>.
- [6] C. Noé, S. Malburet, A. Bouvet-Marchand, A. Graillot, C. Loubat, M. Sangermano, Cationic photopolymerization of bio-renewable epoxidized monomers, *Prog. Org. Coat.* 133 (2019) 131–138, <https://doi.org/10.1016/j.porgcoat.2019.03.054>.
- [7] S.G. Tan, W.S. Chow, Biobased epoxidized vegetable oils and its greener epoxy blends: a review, *Polym.-Plast. Technol. Eng.* 49 (2010) 1581–1590, <https://doi.org/10.1080/03602559.2010.512338>.
- [8] M. Sangermano, N. Razza, J.V. Crivello, Cationic UV-curing: technology and applications, *Macromol. Mater. Eng.* 299 (2014) 775–793, <https://doi.org/10.1002/mame.201300349>.
- [9] M. Sangermano, I. Roppolo, M. Messori, UV-cured functional coatings, in: A. Tiwari (Ed.), *Photocured Materials*, RSC, London, 2014, pp. 121–133, <https://doi.org/10.1039/9781782620075-00121>.
- [10] L. Pezzana, G. Melilli, N. Guigo, N. Sbirrazzuoli, M. Sangermano, Cross-linking of biobased monofunctional furan epoxy monomer by two steps process, UV irradiation and thermal treatment, *Macromol. Chem. Phys.* 224 (2023) 2200012, <https://doi.org/10.1002/macp.202200012>.
- [11] M. Faccini, L. Bautista, L. Soldi, A.M. Escobar, M. Altavilla, M. Calvet, A. Domènech, E. Domínguez, Environmentally friendly anticorrosive polymeric coatings, *Appl. Sci.* 11 (2021) 3446, <https://doi.org/10.3390/app11083446>.
- [12] J.V. Crivello, J.H.W. Lam, Diaryliodonium salts. A new class of photoinitiators for cationic polymerization, *Macromolecules* 10 (1977) 1307–1315, <https://doi.org/10.1021/ma60060a028>.
- [13] C. Noé, M. Hakkarainen, M. Sangermano, Cationic UV-curing of epoxidized biobased resins, *Polymers (Basel)* 13 (2020) 89, <https://doi.org/10.3390/polym13010089>.
- [14] J.V. Crivello, R. Narayan, Epoxidized triglycerides as renewable monomers in photoinitiated cationic polymerization, *Chem. Mater.* 4 (1992) 692–699, <https://doi.org/10.1021/cm00021a036>.
- [15] J.V. Crivello, R. Narayan, S.A. Bratslavsky, B. Yang, The synthesis and cationic polymerization of novel monomers from renewable sources, *Macromol. Symp.* 107 (1996) 75–83, <https://doi.org/10.1002/masy.19961070109>.
- [16] E.A. Baroncini, S. Kumar Yadav, G.R. Palmese, J.F. Stanzione, Recent advances in bio-based epoxy resins and bio-based epoxy curing agents, *J. Appl. Polym. Sci.* 133 (2016), <https://doi.org/10.1002/app.44103>.
- [17] E. Sharmin, F. Zafar, D. Akram, M. Alam, S. Ahmad, Recent advances in vegetable oils based environment friendly coatings: a review, *Ind. Crop. Prod.* 76 (2015) 215–229, <https://doi.org/10.1016/j.indcrop.2015.06.022>.
- [18] R.A. Ortiz, D.P. López, M. de L.G. Cisneros, J.C.R. Valverde, J.V. Crivello, A kinetic study of the acceleration effect of substituted benzyl alcohols on the cationic photopolymerization rate of epoxidized natural oils, *Polymer (Guildf)* 46 (2005) 1535–1541, <https://doi.org/10.1016/j.polymer.2004.12.020>.
- [19] A.F. Saleh, E. Kamarudin, A.B. Yaacob, A.W. Yusoff, M.A. Abdullah, Optimization of biomethane production by anaerobic digestion of palm oil mill effluent using response surface methodology, *Asia Pac. J. Chem. Eng.* 7 (2012) 353–360, <https://doi.org/10.1002/apj.550>.
- [20] M.-A. Tehfe, J. Lalevée, D. Gigmes, J.P. Fouassier, Green chemistry: sunlight-induced cationic polymerization of renewable epoxy monomers under air, *Macromolecules* 43 (2010) 1364–1370, <https://doi.org/10.1021/ma9025702>.
- [21] S.F. Thames, H. Yu, R. Subramanian, Cationic ultraviolet curable coatings from castor oil, *J. Appl. Polym. Sci.* 77 (2000) 8–13, [https://doi.org/10.1002/\(SICI\)1097-4628\(20000705\)77:1%3C8::AID-APP2%3E3.0.CO;2-A](https://doi.org/10.1002/(SICI)1097-4628(20000705)77:1%3C8::AID-APP2%3E3.0.CO;2-A).
- [22] S. Ammar, A.W.M. Illing, K. Ramesh, S. Ramesh, Development of fully organic coating system modified with epoxidized soybean oil with superior corrosion protection performance, *Prog. Org. Coat.* 140 (2020) 105523, <https://doi.org/10.1016/j.porgcoat.2019.105523>.
- [23] C. Decker, T. Nguyen Thi Viet, H. Pham Thi, Photoinitiated cationic polymerization of epoxides, *Polym. Int.* 50 (2001) 986–997, <https://doi.org/10.1002/pi.730>.
- [24] X. Wang, J. Zhang, J. Liu, J. Luo, Phytic acid-based adhesion promoter for UV-curable coating: high performance, low cost, and eco-friendliness, *Prog. Org. Coat.* 167 (2022) 106834, <https://doi.org/10.1016/j.porgcoat.2022.106834>.
- [25] K. Zhang, T. Li, T. Zhang, C. Wang, C. Wang, M. Wu, Adhesion improvement of UV-curable ink using silane coupling agent onto glass substrate, *J. Adhes. Sci. Technol.* 27 (2013) 1499–1510, <https://doi.org/10.1080/01694243.2012.746159>.
- [26] K.-H. Kuo, W.-Y. Chiu, K.-H. Hsieh, Synthesis of UV-curable silane-coupling agent as an adhesion promoter, *Mater. Chem. Phys.* 113 (2009) 941–945, <https://doi.org/10.1016/j.matchemphys.2008.08.071>.
- [27] M.N. Sathyanarayana, M. Yaseen, Role of promoters in improving adhesions of organic coatings to a substrate, *Prog. Org. Coat.* 26 (1995) 275–313, [https://doi.org/10.1016/0300-9440\(95\)00572-2](https://doi.org/10.1016/0300-9440(95)00572-2).
- [28] C. Deyá, Epoxysilane as adhesion promoter in duplex system, *J. Adhes. Sci. Technol.* 27 (2013) 1548–1562, <https://doi.org/10.1080/01694243.2012.747728>.
- [29] W.-S. Kim, J.-J. Lee, Adhesion strength and fatigue life improvement of co-cured composite/metal lap joints by silane-based interphase formation, *J. Adhes. Sci. Technol.* 21 (2007) 125–140, <https://doi.org/10.1163/156856107780437462>.

- [30] E.M. Petrie, Silanes as primers and adhesion promoters for metal substrates, *Met. Finish.* 105 (2007) 85–93, [https://doi.org/10.1016/S0026-0576\(07\)80186-3](https://doi.org/10.1016/S0026-0576(07)80186-3).
- [31] J.H. Waite, Mussel adhesion – essential footnote, *J. Exp. Biol.* 220 (2017) 517–530, <https://doi.org/10.1242/jeb.134056>.
- [32] Y.K. Jeong, S.H. Park, J.W. Choi, Mussel-inspired coating and adhesion for rechargeable batteries: a review, *ACS Appl. Mater. Interfaces* 10 (2018) 7562–7573, <https://doi.org/10.1021/acsami.7b08495>.
- [33] R. Sesia, S. Spriano, M. Sangermano, S. Ferraris, Natural polyphenols and the corrosion protection of steel: recent advances and future perspectives for green and promising strategies, *Metals (Basel)* 13 (2023) 1070, <https://doi.org/10.3390/met13061070>.
- [34] L.Q. Xu, K.-G. Neoh, E.-T. Kang, Natural polyphenols as versatile platforms for material engineering and surface functionalization, *Prog. Polym. Sci.* 87 (2018) 165–196, <https://doi.org/10.1016/j.progpolymsci.2018.08.005>.
- [35] C. Reggio, J. Barberi, S. Ferraris, S. Spriano, Functionalization of Ti6Al4V alloy with polyphenols: the role of the titanium surface features and the addition of calcium ions on the adsorption mechanism, *Metals (Basel)* 13 (2023) 1347, <https://doi.org/10.3390/met13081347>.
- [36] G. Ricucci, S. Ferraris, C. Reggio, A. Bosso, G. Örlgsson, C.H. Ng, S. Spriano, Polyphenols from grape pomace: functionalization of chitosan-coated hydroxyapatite for modulated swelling and release of polyphenols, *Langmuir* 37 (2021) 14793–14804, <https://doi.org/10.1021/acs.langmuir.1c01930>.
- [37] M. Andjelković, J. Van Camp, B. De Meulenaer, G. Depaemelaere, C. Socaciu, M. Verloo, R. Verhe, Iron-chelation properties of phenolic acids bearing catechol and galloyl groups, *Food Chem.* 98 (2006) 23–31, <https://doi.org/10.1016/j.foodchem.2005.05.044>.
- [38] A.-K. Koopmann, C. Schuster, J. Torres-Rodríguez, S. Kain, H. Pertl-Obermeyer, A. Petutschnigg, N. Hüsing, Tannin-based hybrid materials and their applications: a review, *Molecules* 25 (2020) 4910, <https://doi.org/10.3390/molecules25214910>.
- [39] R. Sesia, S. Ferraris, M. Sangermano, S. Spriano, UV-cured chitosan-based hydrogels strengthened by tannic acid for the removal of copper ions from water, *Polymers (Basel)* 14 (2022) 4645, <https://doi.org/10.3390/polym14214645>.
- [40] J. Gust, J. Suwalski, Use of Mössbauer spectroscopy to study reaction products of polyphenols and Iron compounds, *Corrosion* 50 (1994) 355–365, <https://doi.org/10.5006/1.3294344>.
- [41] G. Matamala, W. Smeltzer, G. Drogue, Use of tannin anticorrosive reaction primer to improve traditional coating systems, *Corrosion* 50 (1994) 270–275, <https://doi.org/10.5006/1.3294333>.
- [42] T.S. Sileika, D.G. Barrett, R. Zhang, K.H.A. Lau, P.B. Messersmith, Colorless multifunctional coatings inspired by polyphenols found in tea, chocolate, and wine, *Angew. Chem. Int. Ed.* 52 (2013) 10766–10770, <https://doi.org/10.1002/anie.201304922>.
- [43] C. Byrne, O. D'Alessandro, G.J. Selmi, R. Romagnoli, C. Deyá, Primers based on tara and quebracho tannins for poorly prepared steel surfaces, *Prog. Org. Coat.* 130 (2019) 244–250, <https://doi.org/10.1016/j.porgcoat.2019.02.003>.
- [44] A. Hadzich, S. Flores, J. Caprari, R. Romagnoli, Study of zinc tannates prepared with Tara powder (*Caesalpinia spinosa*) as anticorrosive pigments in alkyd paints and wash primer formulations, *Prog. Org. Coat.* 117 (2018) 35–46, <https://doi.org/10.1016/j.porgcoat.2017.12.019>.
- [45] J. Ramírez, A. Díaz-Gómez, L.F. Montoya, S.S. Samhitha, D. Rojas, Á. Oñate, A. F. Jaramillo, M.F. Melendrez, Evaluation in real conditions of new anticorrosive formulations based on polyphenols from natural sources and encapsulated nanoparticles, *Coatings* 13 (2022) 8, <https://doi.org/10.3390/coatings13010008>.
- [46] O.R. Pardini, J.I. Amalvy, A.R. Sarli, R. Romagnoli, V.F. Vetere, Formulation and testing of a waterborne primer containing chestnut tannin, *J. Coatings Technol.* 73 (2001) 99–106, <https://doi.org/10.1007/BF02698435>.
- [47] J.I. Amalvy, A.C. Aznar, O.R. Pardini, G.A. Guzmán, Waterborne anticorrosive systems for steel protection—part 1: formulation and testing, *Corrosion* 58 (2002) 871–880, <https://doi.org/10.5006/1.3287672>.
- [48] G. Sekaran, S. Thamizharasi, T. Ramasami, Physicochemical and thermal properties of phenol-formaldehyde-modified polyphenol impregnate, *J. Appl. Polym. Sci.* 81 (2001) 1567–1571, <https://doi.org/10.1002/app.1586>.
- [49] G. Matamala, W. Smeltzer, G. Drogue, Comparison of steel anticorrosive protection formulated with natural tannins extracted from acacia and from pine bark, *Corros. Sci.* 42 (2000) 1351–1362, [https://doi.org/10.1016/S0010-938X\(99\)00137-7](https://doi.org/10.1016/S0010-938X(99)00137-7).
- [50] X. Wang, J. Zhang, J. Liu, R. Liu, J. Luo, Synthesis of acrylated tannic acid as bio-based adhesion promoter in UV-curable coating with improved corrosion resistance, *Colloids Surf. A Physicochem. Eng. Asp.* 644 (2022) 128834, <https://doi.org/10.1016/j.colsurfa.2022.128834>.
- [51] A. Alaoui Mouayd, M.E. Orazem, E.M.M. Sutter, B. Tribollet, A. Koltsov, Contribution of electro-chemical dissolution during pickling of low carbon steel in acidic solutions, *Corros. Sci.* 82 (2014) 362–368, <https://doi.org/10.1016/j.corsci.2014.01.036>.
- [52] O. Bezsonov, O. Ilyunin, B. Kaldybaeva, O. Selyakov, O. Perevertaylenko, A. Khusanov, O. Rudenko, S. Udovenko, A. Shamraev, V. Zorenko, Resource and energy saving neural network-based control approach for continuous carbon steel pickling process, *J. Sustain. Dev. Energy Water Environ. Syst.* 7 (2019) 275–292, <https://doi.org/10.13044/j.sdewes.d6.0249>.
- [53] S. Hooshmand Zaferani, M. Sharifi, D. Zaarei, M.R. Shishesaz, Application of eco-friendly products as corrosion inhibitors for metals in acid pickling processes – a review, *J. Environ. Chem. Eng.* 1 (2013) 652–657, <https://doi.org/10.1016/j.jece.2013.09.019>.
- [54] Y. Sun, T. Bell, Plasma surface engineering of low alloy steel, *Mater. Sci. Eng. A* 140 (1991) 419–434, [https://doi.org/10.1016/0921-5093\(91\)90458-Y](https://doi.org/10.1016/0921-5093(91)90458-Y).
- [55] A.S. Katsigiannis, D.L. Bayliss, J.L. Walsh, Cold plasma decontamination of stainless steel food processing surfaces assessed using an industrial disinfection protocol, *Food Control* 121 (2021) 107543, <https://doi.org/10.1016/j.foodcont.2020.107543>.
- [56] S. Pradheebha, R. Unnikannan, R.N. Bathe, G. Padmanabham, R. Subasri, Effect of plasma pretreatment on durability of sol-gel superhydrophobic coatings on laser modified stainless steel substrates, *J. Adhes. Sci. Technol.* 32 (2018) 2394–2404, <https://doi.org/10.1080/01694243.2018.1482735>.
- [57] Z. Zhai, L. Feng, Effect of oxygen plasma treatment on bonding strength of epoxy coating on steel substrate, *Prog. Org. Coat.* 131 (2019) 36–41, <https://doi.org/10.1016/j.porgcoat.2019.02.011>.
- [58] S. Malburet, C. Di Mauro, C. Noé, A. Mija, M. Sangermano, A. Graillet, Sustainable access to fully biobased epoxidized vegetable oil thermoset materials prepared by thermal or UV-cationic processes, *RSC Adv.* 10 (2020) 41954–41966, <https://doi.org/10.1039/D0RA07682A>.
- [59] S. Ferraris, M. Prato, C. Vineis, A. Varesano, G. Gautier di Confengo, S. Spriano, Coupling of keratin with titanium: a physico-chemical characterization of functionalized or coated surfaces, *Surf. Coat. Technol.* 397 (2020) 126057, <https://doi.org/10.1016/j.surfcoat.2020.126057>.
- [60] M. Yoshinari, T. Hayakawa, K. Matsuzaka, T. Inoue, Y. Oda, M. Shimono, T. Ide, T. Tanaka, Oxygen plasma surface modification enhances immobilization of simvastatin acid, *Biomed. Res.* 27 (2006) 29–36, <https://doi.org/10.2220/biomedres.27.29>.
- [61] C. Noé, L. Iannucci, S. Malburet, A. Graillet, M. Sangermano, S. Grassini, New UV-curable anticorrosion coatings from vegetable oils, *Macromol. Mater. Eng.* 306 (2021) 2100029, <https://doi.org/10.1002/mame.202100029>.
- [62] X. Ren, T. Xu, J. Thomas, M.D. Soucek, Isoprene soya diols-alder adduct and epoxidation for photopolymerization, *Macromol. Chem. Phys.* 222 (2021) 2100054, <https://doi.org/10.1002/macp.202100054>.
- [63] L. Pezzana, G. Melilli, P. Delliere, D. Moraru, N. Guigo, N. Sbirrazzuoli, M. Sangermano, Thiol-ene biobased networks: furan allyl derivatives for green coating applications, *Prog. Org. Coat.* 173 (2022) 107203, <https://doi.org/10.1016/j.porgcoat.2022.107203>.
- [64] D3363, Standard Test Method for Film Hardness by Pencil Test, 2011.
- [65] A956/A956M, Standard Test Method for Leeb Hardness Testing of Steel Products, 2017.
- [66] BS EN ISO 2409:2020, Paints and Varnishes, Cross-Cut Test, 2020.
- [67] C. Noé, S. Malburet, E. Milani, A. Bouvet-Marchand, A. Graillet, M. Sangermano, Cationic UV-curing of epoxidized cardanol derivatives, *Polym. Int.* 69 (2020) 668–674, <https://doi.org/10.1002/pi.6031>.
- [68] L. Pezzana, G. Melilli, N. Guigo, N. Sbirrazzuoli, M. Sangermano, Cationic UV curing of bioderived epoxy furan-based coatings: tailoring the final properties by in situ formation of hybrid network and addition of monofunctional monomer, *ACS Sustain. Chem. Eng.* 9 (2021) 17403–17412, <https://doi.org/10.1021/acssuschemeng.1c06939>.
- [69] J.V. Crivello, R. Acosta Ortiz, Benzyl alcohols as accelerators in the photoinitiated cationic polymerization of epoxide monomers, *J. Polym. Sci. A Polym. Chem.* 40 (2002) 2298–2309, <https://doi.org/10.1002/pola.10311>.
- [70] J.V. Crivello, S. Liu, Photoinitiated cationic polymerization of epoxy alcohol monomers, *J. Polym. Sci. A Polym. Chem.* 38 (2000) 389–401, [https://doi.org/10.1002/\(SICI\)1099-0518\(20000201\)38:3%3C389::AID-POLA1%3E3.0.CO;2-G](https://doi.org/10.1002/(SICI)1099-0518(20000201)38:3%3C389::AID-POLA1%3E3.0.CO;2-G).
- [71] S.P. Pappas, Radiation curing—a personal perspective, in: S.P. Pappas (Ed.), *Radiation Curing: Science and Technology*, Springer, New York, 1992, pp. 1–18, <https://doi.org/10.1007/978-1-4899-0712-7>.
- [72] M. Sangermano, Advances in cationic photopolymerization, *Pure Appl. Chem.* 84 (2012) 2089–2101, <https://doi.org/10.1351/PAC-CON-12-04-11>.
- [73] A. Cosola, R. Conti, H. Grützmacher, M. Sangermano, I. Roppolo, C.F. Pirri, A. Chiappone, Multiacrylated cyclodextrin: a bio-derived photocurable macromer for VAT 3D printing, *Macromol. Mater. Eng.* 305 (2020) 2000350, <https://doi.org/10.1002/mame.202000350>.